DALTON
FULL PAPER

Reactions of P_4 and I_2 with $Ag[Al(OC(CF_3)_3)_4]$: from elusive polyphosphorus cations to subvalent $P_3I_6^+$ and phosphorus rich $P_5I_2^+$ †

Ingo Krossing

University of Karlsruhe, Engesserstr. Geb. 30.45, 76128 Karlsruhe, Germany. E-mail: krossing@chemie.uni-karlsruhe.de

Received 3rd May 2001, Accepted 5th November 2001
First published as an Advance Article on the web 29th January 2002

Reactions of X_2 (X = Br, I), P_4 and $Ag(CH_2Cl_2)[Al(OR)_4]$ [R = $C(CF_3)_3$] in suitable ratios to prepare naked polyphosphorus cations were carried out and led to products which suggested the presence of these elusive cations as intermediates. At temperatures above −30 °C to rt the initially formed cations decomposed the $Al(OR)_4^-$ anion giving, in two cases, the more stable fluoride bridged $(RO)_3Al–F–Al(OR)_3^-$ anion. When Br_2 was used as the oxidising agent the proposed intermediate phosphorus cation (P_5^+?) reacted with the solvent $CDCl_3$ by double insertion of a P^+ unit into the C–Cl bond giving $Cl_2P(CDCl_2)_2[(RO)_3Al–F–Al(OR)_3]$, **1**. When I_2 was used as the oxidiser the reaction led to the marginally stable $P_3I_6[(RO)_3Al–F–Al(OR)_3]$, **2** (X-ray). By using very mild conditions throughout (−80 °C) the primary product of the reaction of $Ag(P_4)_2[Al(OR)_4]$ and I_2 was isolated: $P_5I_2[Al(OR)_4]$, **3**, containing the $P_5I_2^+$ cation with a hitherto unknown C_{2v}-symmetric P_5 cage as structural building block. $P_3I_6[Al(OR)_4]$, **4**, was directly synthesised in quantitative yield starting from P_2I_4, PI_3 and $Ag(CH_2Cl_2)[Al(OR)_4]$ in CH_2Cl_2 solution. $P_3I_6^+$ is formed through the $P_2I_5^+$ stage (^{31}P-NMR). $P_3I_6^+$ (av.: $P^{2.33}$) is the first subvalent P–X cation (X = H, F, Cl, Br, I). $P_5I_2^+$ (av.: $P^{0.6}$) is the first phosphorus rich binary P–X cation. They are the third and fourth example of a binary P–X cation after the known PX_4^+ and $P_2X_5^+$ cations. The observed reactions were fully accounted for by thermochemical Born–Haber cycles based on (RI-)MP2/TZVPP *ab initio*, COSMO solvation and lattice enthalpy calculations (all phases). The gaseous enthalpies of formation of several species were calculated to be (in kJ mol^{-1}): P_5^+ (913), $P_3I_6^+$ (694), $P_5I_2^+$ (792), $P_2I_5^+$ (733), $Ag(P_4)_2^+$ (784).

Introduction

Phosphorus, arsenic and fluorine are the only electronegative non-metallic elements for which homopolyatomic elemental cations are still unknown as "compounds in the bottle". For P and As this appears rare, since gaseous phosphorus and arsenic cations are well investigated by mass spectrometric measurements (up to P_{89}^+),[1,2] photo ionisation studies (E_{2-5}^+, E = P, As)[3] and theoretical investigations.[1c,4] Many of the basic thermodynamic properties of E_n^+ (*i.e.* IP's, $\Delta_f H$) are known.[5] (Radical-)Cations E_n^+ with an even number, *n*, of elemental atoms were shown to be considerably less stable than the diamagnetic uneven species E_n^+.[4] However, earlier work showed that classical approaches to salts of E_n^+ (*i.e.* oxidation of E by MF_5 or $F_2S_2O_6$, M = As, Sb) did not lead to success but rather to a decomposition of the anions and formation of E–O and E–F species.[6] And, indeed, the strengths of the E–F bonds (484 and 490 kJ mol^{-1} in EF_3)[5] are amongst the highest known in the periodic table and therefore account for the decomposition reactions. To circumvent the decomposition of the anions, we employed a new generation of weakly basic anions of type $Al(OR)_4^-$ [R = $C(CF_3)_3$], the syntheses of lithium and silver salts of which was recently published by Strauss[7] and us.[8] $Al[OC(CF_3)_3]_4^-$ also appeared to be an ideal spectator ion, since it stabilises the unusual D_{2h} symmetric homoleptic $Ag(P_4)_2^+$ cation.[9] Previously we showed[8] that the $Al[OC(CF_3)_3]_4^-$ anion, which is stable in 35% HNO_3, is one of the most weakly coordinating anions known. Herein we present the results of our efforts to oxidise the silver-P_4 adducts[9] with halogens that finally led to the formation of salts of the $P_3I_6^+$ and $P_5I_2^+$ cations. A preliminary account on $P_5I_2^+$ has been given.[10]

† Electronic supplementary information (ESI) available: a drawing of the single piece apparatus used for the reactions. See http://www.rsc.org/suppdata/dt/b1/b103957c/

Results

Syntheses and spectroscopic characterisation

Initial reactions of $Li[Al(OR)_4]$, P_4 and iodine [R = $C(CF_3)_3$] in various solvents in suitable ratios for the preparation of P_5^+ only led to an orange–red solid material, which, according to the Raman spectra, did not contain the anion but rather was a mixture of red phosphorus and P_2I_4. This was attributed to the very hard and polarising Li^+ cation that, with the reaction conditions employed, didn't react with the soft phosphorus iodides. However, when exchanging Li^+ for Ag^+ and I_2 for Br_2 an ionisation occurred as shown by the NMR scale reaction of $Ag(CH_2Cl_2)[Al(OR)_4]$, 5/4 P_4 and 0.5 Br_2 in $CDCl_3$ [see eqn. (1)]:

$$Ag(CH_2Cl_2)[Al(OR)_4] + 5/4\ P_4 + 0.5\ Br_2 \longrightarrow\longrightarrow Cl_2P(CDCl_2)_2[(RO)_3Al–F–Al(OR)_3]\ \mathbf{1} + AgBr + P_4 + ? \quad (1)$$

[R = $C(CF_3)_3$]

The unit cell of several of the uniform colourless crystals of this reaction was determined and all of them showed the same triclinic cell as **1** indicating that this was the main product of reaction (apart from P_4). The rt ^{31}P-NMR of this solution showed two lines: an intense line attributable to P_4 and another weaker resonance we assign to the $Cl_2P(CDCl_2)_2^+$ cation (144 ppm, *cf.* 96 ppm in $PCl_4^+PCl_6^-$). Presumably a very electrophilic phosphorus cation [*e.g.* P_5^+, *cf.* eqn. (2)] was initially formed

 DOI: 10.1039/b103957c

which decomposed the anion and finally led to the observed products. The formation of the $Cl_2P(CDCl_2)_2^+$ cation in **1** is then seen as a double insertion of a P^+ unit (possibly from P_5^+) into a C–Cl bond (see Discussion).

We concluded that iodine should be a more suitable oxidising agent than bromine since it is solid and reactions are, therefore, slower. A thermochemical evaluation[11,12] of eqn. (2) showed it to be favourable by 149 kJ mol^{-1}:

$$Ag[Al(OR)_4]\ (s) + 5/4\ P_4\ (s) + 0.5\ I_2\ (s) \longrightarrow P_5[Al(OR)_4]\ (s) + AgI\ (s) \quad (2)$$

$[R = C(CF_3)_3]$; $\Delta_rH = -149$ kJ mol^{-1}

More polar solvents such as CH_2Cl_2 (*cf.* ε = 8.9 *vs.* 4.8 for $CHCl_3$)[5c] should also help to stabilise the ions (*cf.* the computational work below). Therefore a reaction as in eqn. (2) was performed in CH_2Cl_2. The reaction temperature in this experiment was always kept below −20 °C and immediately after consumption of all visible amounts of iodine part of the orange coloured solution was poured into a glass tube. All volatiles were then removed *in vacuo* and the Raman spectrum of the remaining orange material showed bands attributable to the intact anion, $Ag(P_4)_2^+$, P_2I_4 but also new P–P stretches that possibly stem from yet unknown phosphorus cations P_n^+ (n = 3, 5, 7).[13] In further reactions according to eqn. (2) the presence of larger amounts of P_2I_4 was reinforced by the isolation of orange triclinic crystals which, according to their unit cell[14] and Raman spectrum, were P_2I_4. Therefore P_2I_4 appeared to be a thermodynamic sink in this reaction. To exploit the formation of P_2I_4 as an additional driving force the underlying thermochemistry[11] was examined in a suitable cycle [see eqn. (3)].

$$Ag[Al(OR)_4]\ (s) + 2\ P_4\ (s) + 3.5\ I_2\ (s) \longrightarrow P_5[Al(OR)_4]\ (s) + 1.5\ P_2I_4\ (s) + AgI\ (s) \quad (3)$$

$[R = C(CF_3)_3]$; $\Delta_rH = -287$ kJ mol^{-1}

Indeed we found that eqn. (3) should be considerably more favourable than a reaction according to eqn. (2) {Δ_rH [eqn. (3)] = −287 kJ mol^{-1} *vs.* Δ_rH [eqn. (2)] = −149 kJ mol^{-1}}. Consequently eqn. (3) was initially performed in CH_2Cl_2 and after stirring the reaction mixture overnight at −30 °C all volatiles were removed. To extract the very CS_2 soluble by-product, P_2I_4, the solid yellow–orange residue was extracted with CS_2 at rt[15] and, to our surprise, much of the solid material was soluble in this very non-polar solvent. From the concentrated CS_2 solution of this reaction we obtained a mixture of single crystals. Amongst orange P_2I_4 needles (unit cell determination[14] and Raman) a larger amount of yellow plate-like and extremely sensitive crystals was found and the single crystal X-ray structure determination of these yellow plates showed them to be $P_3I_6[(RO)_3Al–F–Al(OR)_3]$, **2**, containing the first subvalent binary P–X cation (X = H, F, Cl, Br, I) with an average oxidation state of P of 2.33. In the ^{31}P-NMR of this CS_2 solution lines attributable to PI_3 and P_2I_4 appeared at $\delta^{31}P$ = 176 and 105 but were very broad ($\nu_{1/2}$ = 2100 and 1600 Hz) indicating rapid exchange (with $P_3I_6^+$?). Repeating the ^{31}P-NMR spectra at low temperature (−30 and −70 °C) led to sharp lines ($\nu_{1/2}$ = 5 Hz) with greatly enhanced signal-to-noise ratio at the expected positions for PI_3 and P_2I_4 at $\delta^{31}P$(−30 °C and −70 °C) = 176 and 105, but no additional lines due to a P-containing cation emerged—indicating that the cation had precipitated or that a fast exchange between the unknown species ($P_3I_6^+$?) and PI_3, P_2I_4 or the solvent was still occuring. The overall reaction with all observed products is given in eqn. (4):

$$Ag(CH_2Cl_2)[Al(OR)_4] + 2\ P_4 + 3.5\ I_2 \longrightarrow\longrightarrow P_3I_6[(RO)_3Al–F–Al(OR)_3],\ \mathbf{2} + PI_3 + P_2I_4 + AgI + ? \quad (4)$$

$[R = C(CF_3)_3]$

The obtained $P_3I_6^+$ salt was always contaminated with the very intense Raman scatterer P_2I_4 which prevented its Raman observation, however, we succeeded in the independent direct synthesis of $P_3I_6^+$ (see below).

We reinvestigated the reaction as proposed in eqn. (3) by low temperature *in situ* NMR spectroscopy but using pure $[Ag(P_4)_2][Al(OR)_4]$[9] instead of the $Ag(CH_2Cl_2)[Al(OR)_4]$/2 P_4 mixture. When $[Ag(P_4)_2][Al(OR)_4]$[9] in CD_2Cl_2 was reacted with 3.5 equivalents of I_2 at −78 °C one major product was observed in the *in situ* ^{31}P-NMR spectrum (−90 °C) recorded after 30 minutes: $[P_5I_2][Al(OR)_4]$ **3** [eqn. (5)] containing a C_{2v}-symmetric $P_5I_2^+$ cation, the *in situ* ^{31}P-NMR spectrum of which is shown in Fig. 1.

Both pure PI_3 and P_2I_4 are insoluble in CD_2Cl_2 at these temperatures (^{31}P-NMR) and, therefore, exchange with the cation as in CS_2 did not occur. Small amounts of solid P_4 were also visible in the ^{31}P-NMR (not shown).[16] A larger preparative reaction, always kept at −80 °C, verified these conclusions based on the mass balance, the Raman observation of pure $P_5I_2^+[Al(OR)_4^-]$ **3** in the soluble and PI_3, P_4 and traces of P_2I_4 in the insoluble material of this reaction as well as an elemental analysis of **3**. The balanced overall reaction with the observed products is given in eqn. (5):

$$[Ag(P_4)_2^+][A^-] + 3.5\ I_2 \xrightarrow[CD_2Cl_2]{-78°C,} [P_5I_2^+][A^-] + AgI + 4/3PI_3 + 5/12P_4 \quad (5)$$

$$\downarrow\ T > -40°C$$

$[A^-] = Al[OC(CF_3)_3]_4^-$ $\qquad$ $P_3I_6^+ + ?$

Solid pure **3** may be handled at rt for 1–2 hours, however, upon warming the NMR tube overnight to −40 °C the $P_5I_2^+$ signals vanish and, apart from other unassigned signals of lower intensity, those of $P_3I_6^+$ appear as major P-containing peaks (*cf.* $P_3I_6[Al(OR)_4]$, **4**, below). The observation of only traces of P_2I_4 but large amounts of PI_3 in the Raman spectrum, at −80 °C, of the insoluble material of eqn. (5) shows that in the earlier reactions P_2I_4, which was always found, is formed from PI_3 and P_4 *only* upon warming. Initial PI_3 formation is in agreement with Tattershall's[17] earlier observation that P_4 reacts with I_2 to immediately give PI_3 which is then reduced by P_4 giving P_2I_4. From the Raman spectrum[18] of the very air and moisture sensitive solid yellow **3**, shown in Fig. 2, the presence of the intact $Al(OR)_4^-$ anion {796 and 745 cm^{-1}, *cf.* 798 and 746 cm^{-1} in $Ag(P_4)_2[Al(OR)_4]$[9]} as well as a P–I stretch at 168 cm^{-1} immediately follow and support the assignment of the $P_5I_2^+$ cation (see Discussion).

With the awareness of the $P_3I_6^+$ cation we succeeded in directly synthesising this species by reacting PI_3, P_2I_4 and $Ag(CH_2Cl_2)[Al(OR)_4]$ according to eqn. (6).

$$Ag(CH_2Cl_2)[Al(OR)_4] + P_2I_4 + PI_3 \longrightarrow P_3I_6[Al(OR)_4],\ \mathbf{4} + AgI\ [R = C(CF_3)_3] \quad (6)$$

After 12 h at −78 °C the obtained yellow–orange solution (over an AgI precipitate) was investigated by variable temperature ^{31}P-NMR spectroscopy, shown in Fig. 3.

Only at very low temperatures (below −80 °C) was the resolution of the spectra good enough to resolve P–P coupling. $P_3I_6^+$ was identified as main product (62% P), smaller amounts of $P_2I_5^+$ were also visible (28% P).[19] After two weeks storage at −30 °C the $P_2I_5^+$ was no longer visible in the −90 °C ^{31}P-NMR spectrum leaving $P_3I_6^+$ as the only observed P-containing species. This suggests that the formation of $P_3I_6^+$ proceeds through $P_2I_5^+$. The formation of **4** as the only remaining P-containing species according to eqn. (6) was verified in solution (^{31}P-NMR) and solid state (elemental analysis) on a larger

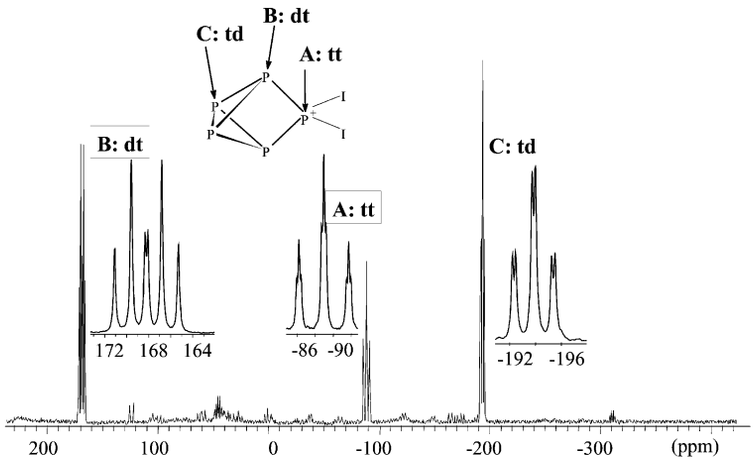

Fig. 1 *In situ* ^{31}P-NMR spectrum of $P_5I_2^+$ in **3** at −90 °C. td = triplet of doublets, dt = doublet of triplets, tt = triplet of triplets.

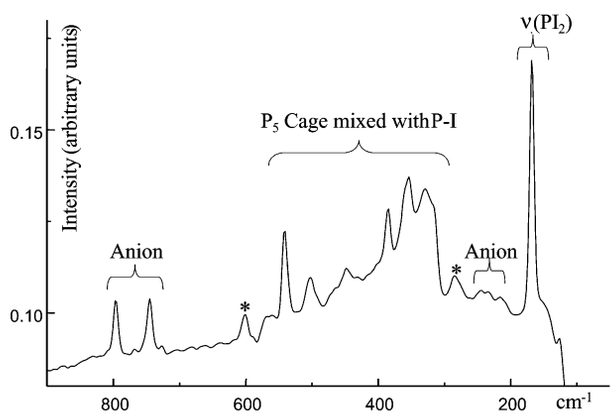

Fig. 2 Raman spectrum of solid **3**. Bands marked with an asterisk show small impurities due to the 100% A_1 breathing modes of the very intense Raman scatterers P_4 (600 cm^{-1}) and PI_3 (284 cm^{-1}).[18]

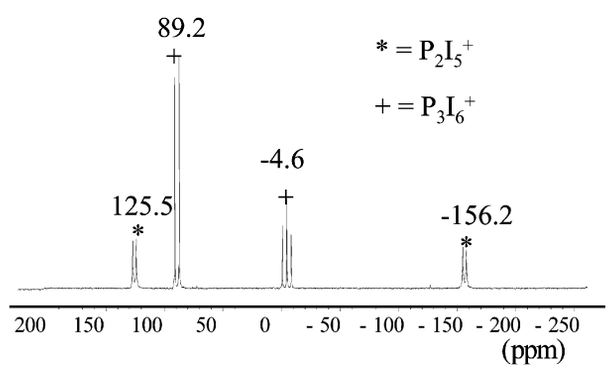

Fig. 3 NMR spectrum of the reaction of 1.0 P_2I_4 + 1.0 PI_3 + 1.0 $Ag[Al(OR)_4]$ after 12 h at −78 °C in CD_2Cl_2 at −90 °C.

preparative scale, however, we were unable to grow single crystals of **4**. Concentrated crystallisation samples always disproportionated giving P_2I_4 and $P_2I_5[Al(OR)_4]$[20] (Raman, unit cell determination). Raman samples prepared from the yellow solid obtained upon removal of all volatiles from the orange–yellow CH_2Cl_2 solution of **4** decomposed rapidly in the beam of the laser (1064 nm) even with wide focus and low laser energy. In CD_2Cl_2 solution the approximately C_2 symmetric $P_3I_6^+$ cation (see X-ray) gave the expected doublet ($\delta^{31}P$ = 89.2, $^1J_{pp}$ = 385.5 Hz) and triplet ($\delta^{31}P$ = −4.6, $^1J_{pp}$ = 385.5 Hz) with a 2 : 1 intensity ratio while the approximately C_s symmetric $P_2I_5^+$ cation[21] gave two doublets at $\delta^{31}P$ = 127.4 and −156.3 with a coupling constant of $^1J_{PP}$ = 320.2 Hz (1 : 1 intensity ratio). In contrast, the $P_2I_5^+$ cation in $P_2I_5AlI_4$ is only stable in the solid state and NMR spectra of CS_2 solutions of the salt showed the signals of PI_3 and AlI_3.[22] The solid state ^{31}P-MAS-NMR spectrum of $P_2I_5AlI_4$[22] showed two broad resonances centred at $\delta^{31}P$ = +114 and −142,[22] confirming the assignment of our solution values.[20]

To determine the activation energy for the exchange between the two different P atoms in $P_3I_6^+$ the coalescence temperature was determined by a series of spectra ran at temperatures between 183 and 298 K (see Fig. 4). Using the Eyring-

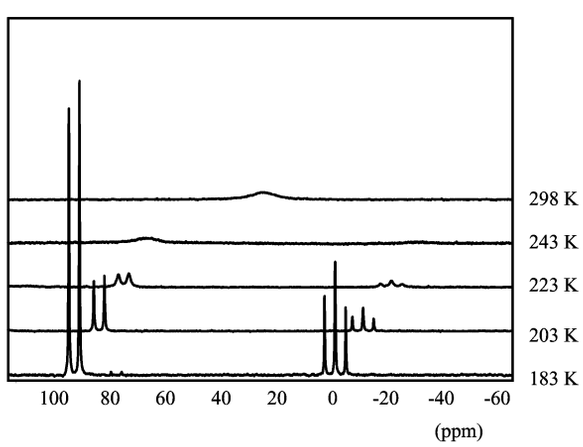

Fig. 4 Spectra of $P_3I_6^+$ between 183 and 298 K; coalescence of $P_3I_6^+$ at 243 K.

equation[23] and the coalescence temperature of 243 K the free energy of activation for the exchange of the two different phosphorus nuclei A and B in I_2P^A–P^BI_2–$P^AI_2^+$ (= $P_3I_6^+$) was estimated as:

$$\Delta G^{\#}(P^A \longrightarrow P^B) = 38.9 \text{ kJ mol}^{-1}$$

Crystal structures

Details on the crystal structure solution and refinement are included in Table 6 (see Experimental).

The $Cl_2P(CDCl_2)_2^+$ cation in 1. Colourless block-like triclinic crystals of **1** (space group $P\bar{1}$) grew in a sealed NMR tube of a NMR-scale reaction. Although the quality of the structure is not very good,[24] the cation—in contrast to the CF_3 groups of the anion—is well behaved with reasonable standard deviations and shall therefore be briefly described (Fig. 5). $Cl_2P(CDCl_2)_2^+$ may be derived from PCl_4^+ by replacing two Cl atoms by

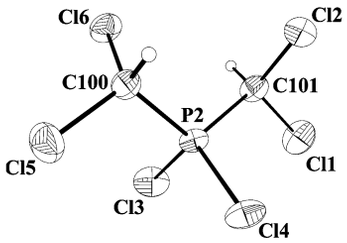

Fig. 5 Geometry of the $Cl_2P(CDCl_2)_2^+$ cation in $Cl_2P(CDCl_2)_2^+$-$[(RO)_3Al–F–Al(OR)_3^-]$, **1**. Anisotropic thermal ellipsoids are drawn at the 25% probability level. Selected bond lengths (Å) and angles (°): P2–Cl3 1.937(3), P2–Cl4 1.938(3), P2–C100 1.818(7), P2–C101 1.835(9), C100–Cl5 1.721(9), C100–Cl6 1.769(9), C101–Cl1 1.756(9), C101–Cl2 1.717(10); Cl3–P2–Cl2 110.0(1), C100–P2–Cl3 108.8(3), C100–P2–Cl4 109.2(3), C101–P2–Cl3 110.2(3), C101–P2–Cl4 108.1(3), C100–P2–C101 110.6(4).

$C(D)Cl_2$ groups to give an almost C_2 symmetric cation with a tetrahedrally coordinated central phosphorus atom. The P–Cl bond lengths [av. 1.938(3) Å] are in the same range as those in the PCl_4^+ cation (1.97 Å) and the bond angles around P2 range from 108.1 to 110.6°. This structure is in very good agreement with a MP2/TZVPP optimisation.[25]

The $P_3I_6^+$ cation in 2. The yellow extremely moisture and oxygen sensitive plates of **2** crystallise in the triclinic space group $P\bar{1}$ with two molecules in the unit cell. The structure of the $P_3I_6^+$ cation shown in Fig. 6 is almost C_2 symmetric and may be described by replacing two iodine atoms of a central PI_4^+ unit by phosphorus linked PI_2 groups. The P–P bond lengths within the P_3 backbone are in the range of normal single bonds [2.210(7) and 2.216(7) Å] and similar to the ones found in $P_2I_5AlI_4$ [2.218(13) Å] or P_2I_4 [2.230(3) Å]. The P–I bond lengths range from 2.361(6) to 2.435(6) Å and are on average 2.393 Å which may be compared to the 2.409 Å (av.) found in $P_2I_5AlI_4$. Two iodine atoms (I1 and I6) with longer P–I distances are involved in intramolecular contacts to P1 and P3 at d(I–P) = 3.621(6) and 3.674(6) Å. The coordination around the central P2 atom is distorted tetrahedral as seen by the range of bond angles of 105.1(2) to 114.9(2)° and the geometry of the two PI_2 units is very similar to that of the PI_2 part in $P_2I_5AlI_4$ [*cf.* $d(P–I)_{av.}$ = 2.398 Å, $(I–P–I)_{av.}$ = 105.3° in **2** and 2.420 and 103.8° in $P_2I_5AlI_4$]. However, compared to P_2I_4 [$d(P–I)_{av.}$ = 2.474 Å] the average P–I distances in **2** are shorter by 0.081 Å.

The $[(RO)_3Al–F–Al(OR)_3]^-$ anions. This bridged anion consists of a linear central Al–F–Al unit [d(Al–F) = 1.760–1.761 Å]. Each Al atom is additionally coordinated by three OR ligands with very short Al–O bond lengths of 1.671 to 1.719 Å. The anions are staggered with respect to the orientation of the two AlO_3 units and in $P_3I_6^+[(RO)_3Al–F–Al(OR)_3]^-$ the central fluorine atom resides on a centre of inversion (see Fig. 7).

The structural parameters of the two anions are summarised in Table 1 and compared to those of the $Al(OR)_4^-$ anion [$Ag(Cl_2C_2H_4)_3^+$ salt].[8]

The average Al–O bond lengths (Al–O–C bond angles) in the fluoride bridged anions are shorter (wider) than those of the homoleptic $Al(OR)_4^-$ anion accounting for the greater electron deficiency of the aluminium centres in **1** and **2**. Therefore, and due to the short Al–F bonds, we propose that the OR ligands in the $(RO)_3Al–F–Al(OR)_3^-$ anions are more tightly bound than in the $Al(OR)_4^-$ anion. The space filling representation (see Fig. 8) of the anion also shows that the bridging fluoride and all oxygen atoms are not accessible and therefore not available for further decomposition reactions.

Solid state packing of 2. 2 forms a layer structure, as shown in Fig. 9, that may formally be derived from a triclinic distorted CsCl structure, *i.e.* the ellipsoidal $(RO)_3Al–F–Al(OR)_3^-$ anions form a (distorted) primitive cubic lattice in which the cations occupy all cubic interstices. The $P_3I_6^+$ cations are linked *via* very weak I–I contacts at 4.070(6) Å and form endless chains along the crystallographic *a*-axis.

Computational results

To verify the nature of the $P_5I_2^+$ and $P_3I_6^+$ cations and to understand the thermodynamics of the formation of the P–I cations,

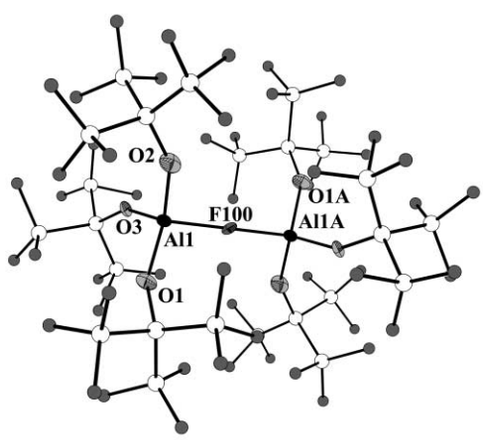

Fig. 7 Structure of the $(RO)_3Al–F–Al(OR)_3^-$ anion in **2**. The oxygen (light grey), aluminium (dark grey) and central fluorine atom(s) are drawn with anisotropic thermal ellipsoids at the 25% probability level. For clarity, all carbon (white) and the remaining fluorine (grey) atoms are drawn as small isotropic circles of arbitrary scale. The geometry of the $(RO)_3Al–F–Al(OR)_3^-$ anion in **1** is similar (see Table 1) and therefore not shown.

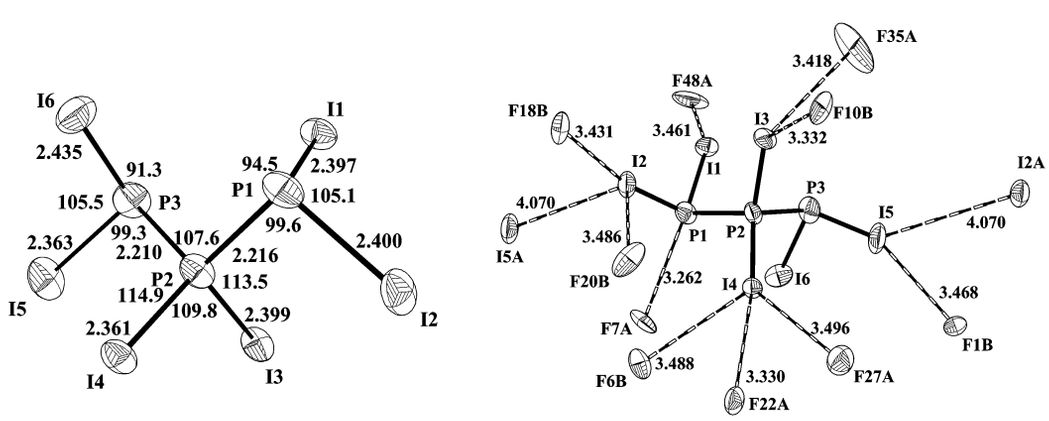

Fig. 6 Geometry and solid state contacts of the $P_3I_6^+$ cation in $P_3I_6^+[(RO)_3Al–F–Al(OR)_3^-]$, **2**. Anisotropic thermal ellipsoids are drawn at the 25% probability level. Selected bond lengths (Å) and angles (°) are given in the figure, standard deviations are 0.006 Å for P–I, 0.007 Å for P–P and 0.2° for the bond angles.

Table 1 Comparison of the structural parameters of the $(RO)_3Al–F–Al(OR)_3^-$ anions in **1**, **2** and the $Al(OR)_4^-$ anion $[Ag(Cl_2C_2H_4)_3^+$ salt]

Parameter	**1**	**2**	$Al(OR)_4^-$
d(Al–O) range/Å	1.681(4)–1.719(5)	1.671(9)–1.700(9)	1.714(3)–1.736(3)
$d(Al–O)_{av.}$/Å	1.692	1.687	1.725
$(Al–O–C)_{av.}$/°	152.8	154.9	149.5
d(Al–F) range/Å	1.761(3)–1.761(3)	1.760(4)–1.761(4)	—
$d(Al–F)_{av.}$/Å	1.761	1.761	—
(Al–F–Al)/°	176.6(2)	180	—

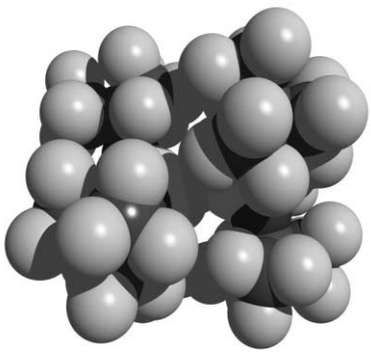

Fig. 8 Space filling representation of the $(RO)_3Al–F–Al(OR)_3^-$ anion.

as opposed to the homopolyatomic phosphorus cations, we fully optimised the geometries of $P_3I_6^+$ (C_2), $P_5I_2^+$ (C_{2v}), $P_2I_5^+$ (C_s), P_2I_4 (C_{2h}), PI_3 (C_s), P_5^+ (C_{4v}), P_4 (T_d), $Ag(P_4)_2^+$ (D_{2h}), I_2 (D_{6h}) and AgI (C_1) at the BP86/SVP, B3LYP/TZVPP and MP2/TZVPP levels. A careful analysis of the computed structural parameters revealed that both pure DFT (BP86) and hybrid HF-DFT (B3LYP) were not capable of reproducing the structural parameters of the experimental geometries. The newer DFT MPWPW91 and, to a lesser extent, the HF-DFT MPW1PW91 levels also failed to give satisfactory geometries. However, at the (RI-)MP2/TZVPP level geometries with structural parameters close to the experimental data were obtained. This may be exemplified by a comparison of the computed and experimental geometries of the $P_2I_5^+$ and $P_3I_6^+$ cations in Table 2.

Table 2 shows that the length of the P–P bond is sensitive to the level of theory chosen and therefore is a good indicator for the quality of the computation. The longest P–P bonds were obtained by BP86/SVP (0.14 to 0.17 Å too long). Only MP2 (and to a lesser extent MPW1PW91) gave acceptable P–P distances that were about 0.03 Å too long. A reason for this discrepancy may be found in the possible interaction of the occupied lone pair orbitals at the iodine atoms [= LP(I)] with the empty (P–P)σ* orbital [= σ*(P–P)] as shown for $P_2I_5^+$ in Fig. 10.

This electron transfer from LP(I) ⟶ σ*(P–P) should considerably elongate the P–P bond but only slightly shorten the P–I bonds. With the basis sets employed DFT and HF-DFT theory appeared to overestimate the interaction, as shown in Fig. 10, and therefore gave very long P–P bonds. Consequently only the structural parameters of the species computed with MP2 were collected in Fig. 11.

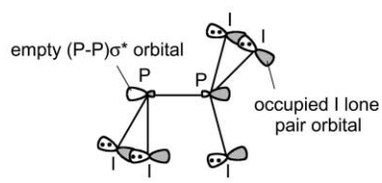

Fig. 10 Possible interaction leading to elongation of the P–P bond in the DFT and HF-DFT optimisations.

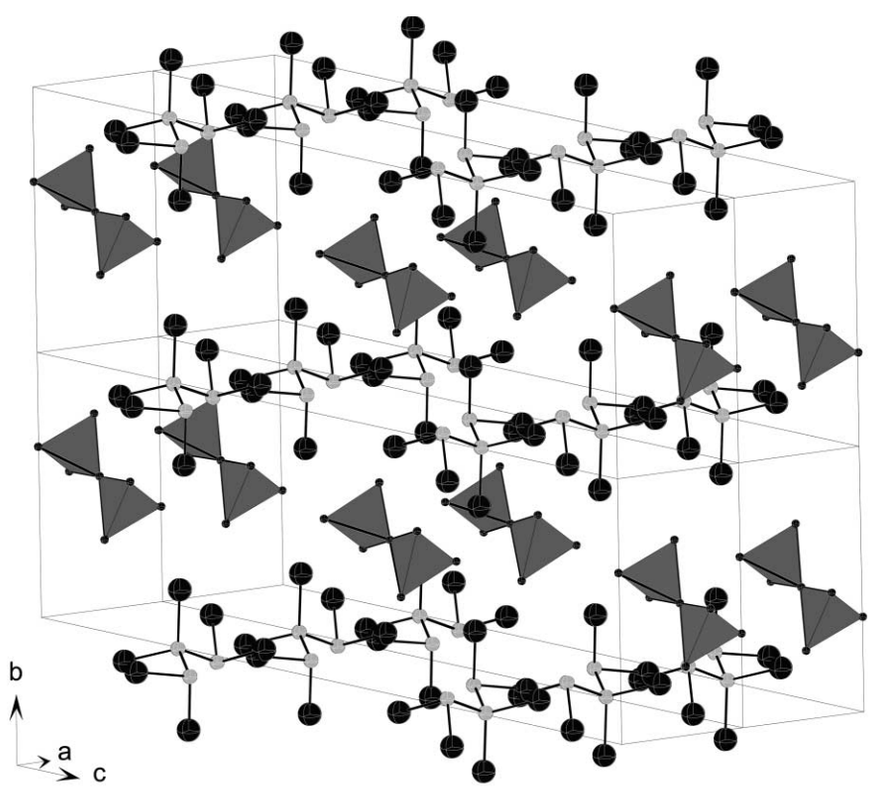

Fig. 9 Solid state packing of **2**. All carbon and fluorine atoms (apart from those in the Al–F–Al linkages) are omitted for clarity. The $F(AlO_3)_2$ units are shown as polyhedra and the cations as ball and stick representations (P: light grey, I: dark grey).

Table 2 Comparison of the computed and experimental geometries of the $P_2I_5^+$ and $P_3I_6^+$ cations. Distances are given in Å

	Exp.$_{(av.)}$ [a]	MP2 [b]	BP86 [c]	B3LYP [b]	MPWPW91 [d]	MPW1PW91 [d]
$P_3I_6^+$						
P–P	2.213	2.247	2.355	2.328	2.315	2.270
I_2P^+(**PI_2**)$_2$	2.415	2.430	2.497	2.464	2.462	2.434
	2.381	2.414	2.469	2.447	2.440	2.420
I_2P^+(PI_2)$_2$	2.379	2.373	2.454	2.422	2.417	2.388
$P_2I_5^+$						
P–P	2.218	2.253	2.390	2.344	—	—
I_3P^+–**PI_2**	2.420	2.413	2.464	2.442	—	—
I_3P^+–PI_2	2.402	2.376	2.458	2.422	—	—

[a] Experimental data stem from the cations in **2** and in $P_2I_5AlI_4$. [b] TZVPP basis set. [c] SVP basis set. [d] 6-311G(2df) for P and SDD(spdf) for I.

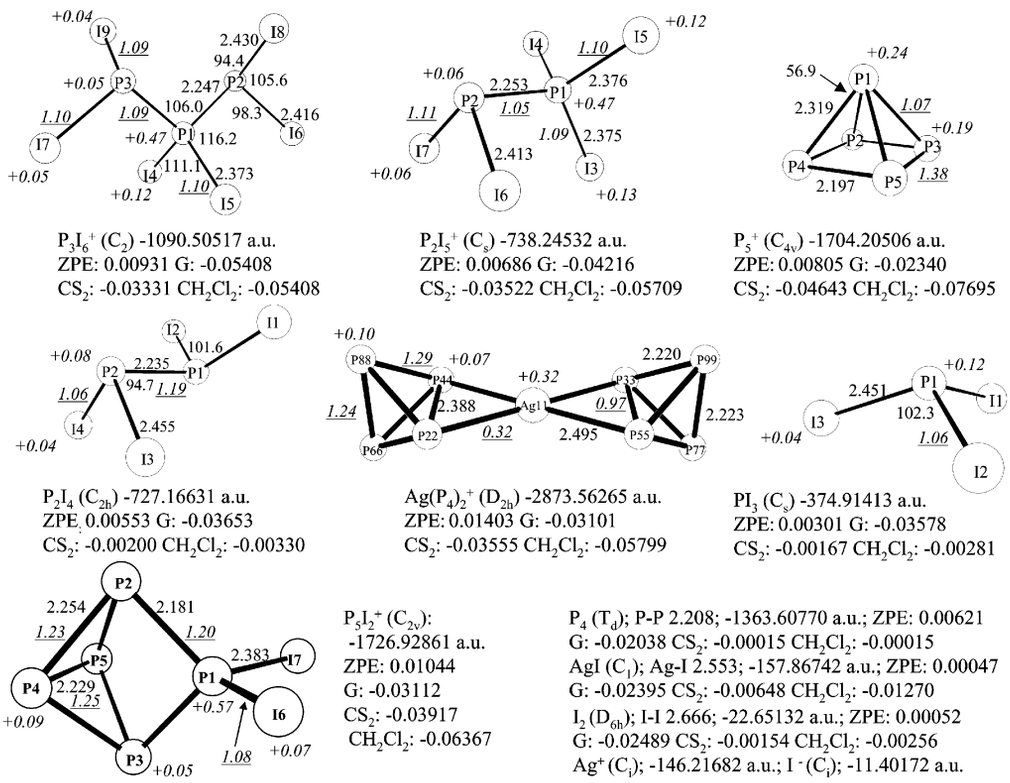

Fig. 11 Fully optimised geometries, atomic energies and zero point energies (= ZPE), thermal corrections[40] to the free enthalpy at 298 K (= *G*), solvation energies[39] in CS_2 (= CS_2) or CH_2Cl_2 (= CH_2Cl_2) of several binary P–I species, $Ag(P_4)_2^+$, P_5^+, P_4, I_2 and AgI at the (RI-)MP2/TZVPP level. Computed partial charges are given in italics, shared electron numbers are shown in italics and underlined. All species included are true minima with no imaginary frequencies.

The quality of the data collected in Fig. 11 is further established by comparison to the experimental geometries of P_4, P_2I_4, PI_3, I_2 and AgI: observed and calculated parameters differ by a maximum of −0.020 Å and +1.1°. The geometries of $Cl_2P(CHCl_2)_2^+$ and $CHCl_3$ were also optimised at the MP2/TZVPP level.[25,26]

Computationally assessed thermochemical properties. For the estimation of thermochemical properties of reactions of the presented species and as an input for Born–Fajans–Haber cycle calculations we derived the enthalpies of formation of several species based on the accurate MP2/TZVPP calculations. For applications see ref. 27. ZPE energies were included in all cases. Known enthalpies of formation were taken from the literature.[5,11] [(g) = gaseous)]

$\Delta_fH(P_5^+$ (g)) followed from the reaction enthalpy of P_3^+ with 0.5 P_4 ($\Delta_rH = -120$ kJ mol^{-1}) as:

$$\Delta_fH(P_5^+ (g)) = \Delta_fH(P_3^+ (g)) + [0.5 \times \Delta_fH(P_4 (g))] - 120 \text{ kJ mol}^{-1}$$
$$= 1006 + (0.5 \times 54) - 120 = \mathbf{913\ kJ\ mol^{-1}}$$

This may be compared to the experimental $\Delta_fH(P_4^+$ (g)) of 942 kJ mol^{-1}.[28] $\Delta_fH(Ag(P_4)_2^+$ (g)) followed from the enthalpy of reaction of $Ag(P_4)_2^+$ (g) giving Ag^+ (g) and 2 P_4 (g) ($\Delta_rH = -341$ kJ mol^{-1}) as:

$$p\Delta_fH(Ag(P_4)_2^+ (g)) = \Delta_fH(Ag^+ (g)) + [2 \times \Delta_fH(P_4 (g))] - 341 \text{ kJ mol}^{-1}$$
$$= 1017 + (2 \times 54) - 341 = \mathbf{784\ kJ\ mol^{-1}}$$

$\Delta_fH(P_3I_6^+$ (g)) followed from the enthalpy of reaction of Ag^+ (g) + 1.5 P_2I_4 (g) + 0.5 I_2 (g) ⟶ $P_3I_6^+$ (g) + AgI (g) ($\Delta_rH = -212$ kJ mol^{-1}) as:

$$\Delta_fH(P_3I_6^+ (g)) = [1.5 \times \Delta_fH(P_2I_{4(g)})] + \Delta_fH(Ag^+_{(g)}) + [0.5 \times \Delta_fH(I_{2(g)})] - \Delta_fH(AgI_{(g)}) - 212 \text{ kJ mol}^{-1}$$
$$= [1.5 \times -4.7] + 1017 + [0.5 \times 62.4] - 135 - 212 = \mathbf{694\ kJ\ mol^{-1}}$$

$\Delta_fH(P_2I_5^+$ (g)) followed from the enthalpy of reaction of eqn. (g) in Table 5 ($\Delta_rH = +45$ kJ mol^{-1}) as:

$$\Delta_f H(P_2I_5^+\,(g)) = \Delta_f H(P_3I_6^+\,(g)) - [0.25 \times \Delta_f H(P_2I_4\,(g))] - [0.125 \times \Delta_f H(P_4\,(g))] + 45\ \text{kJ mol}^{-1}$$
$$= 694 - [0.25 \times -4.7] - [0.125 \times 54] + 45 = \mathbf{733\ kJ\ mol^{-1}}$$

$\Delta_f H(P_5I_2^+\,(g))$ followed from the enthalpy of reaction of eqn. (f) in Table 5 ($\Delta_r H = -49$ kJ mol^{-1}) as:

$$p\Delta_f H(P_5I_2^+\,(g)) = \Delta_f H(P_3I_6^+\,(g)) + \Delta_f H(P_4\,(g)) - \Delta_f H(P_2I_4\,(g)) + 49\ \text{kJ mol}^{-1}$$
$$= 694 + 54 - (-4.7) + 49 = \mathbf{792\ kJ\ mol^{-1}}$$

Discussion

Establishing the nature of $P_5I_2^+$: ^{31}P-NMR and Raman spectra

One comment prior to discussion: It is not adequate to calculate the ^{31}P-NMR chemical shifts of the P–I cations by the standard procedures built in many quantum chemical program codes due to relativistic effects.[29,30] Iodine substituents at tetracoordinate phosphorus atoms lead to a very pronounced relativistic upfield shift that may reach several hundred ppm.[29,30]

The connectivity of the novel P_5 cage within $P_5I_2^+$ followed unequivocally from the coupling pattern and integration of the first order ^{31}P-NMR spectrum (Fig. 1). The C_{2v} symmetric P_5 cage of the cation is without precedence and was not found as part of the many polyphosphides or organopolyphosphanes known to date.[31] However, it still remained to be established that the single phosphorus atom P_A bears two iodine atoms. A P_5^+ cation with the same C_{2v} cage structure could be ruled out based on the calculated high MP2/TZVPP relative energies (including solvation energies) and the calculated ^{31}P-NMR shifts for these species, even when the coordination of one or two molecules of CH_2Cl_2 in several possible geometries was assumed.[32] Moreover C_{2v}-P_5^+ and its CH_2Cl_2 solvates are not true minima but transition states or saddle points with imaginary frequencies (see Fig. 12).[33]

The dicoordinate formally positively charged single P_A atom in C_{2v}-P_5^+ would be expected to resonate somewhere between +1000 and +300 ppm,[32] depending on the number, n, of CH_2Cl_2 molecules in $P_5^+(CH_2Cl_2)_n$ (n = 0, 1, 2, several isomers). However, Table 3 shows that δ^{31}P(P_A in **3**) is at considerably higher field at −89.0 ppm. This is in the middle of the values observed in $P_3I_6^+$ (−4.6 ppm) with two electron-withdrawing PI_2 units attached to P_A and that of P_A in $P_2I_5^+$ which bears a third iodine atom which further shifts[29] the signal to higher field (to −142 or −156.2 ppm, see Table 3). Therefore the position of the electron-rich substituted PI_2^+ unit in $P_5I_2^+$ at δ^{31}P = −89.0 is very reasonable (electron donating bicyclobutane-P_4 moiety). Moreover the rather large $^1J_{PP}$ couplings of the three P_A atoms in the P–I cations are in the same range, *cf.* 278.5 Hz in $P_5I_2^+$, 320.2 Hz in $P_2I_5^+$ and 385.5 Hz in $P_3I_6^+$ (Table 3). The chemical shifts of the atoms of the naked P_4 unit in **3** can only be compared to metal–tetraphosphabicyclobutane

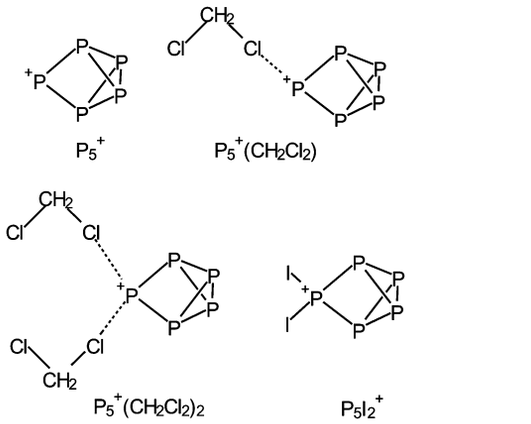

Fig. 12 Computationally assessed possible unsolvated and solvated C_{2v}-P_5^+ structures. Only one of several examined $P_5^+(CH_2Cl_2)_n$ isomers is schematically shown (n = 0, 1, 2).

units since a similar P_5 cage is unknown. However, the electropositive Cp_2M (M = Zr, Hf) groups Z[34] in Table 3 are good substitutes for the PI_2^+ unit in $P_5I_2^+$ and chemical shifts of P_B and P_C as well as the smaller $^1J(P_{BC})$ coupling constants in Cp''_2HfP_4,[34] $Cp^*_2ZrP_4$[34] and $P_5I_2^+$ match very well (Table 3).

Raman spectroscopy is also in agreement with the assignment of **3** as $P_5I_2[Al(OR)_4]$. Observed and calculated vibrational frequencies are in very good agreement and are assigned in Table 4.

The presence of the intact $Al(OR)_4^-$ anion followed from the characteristic bands at 796, 745, 318 and 234 cm^{-1} which are very similar to those observed in $Ag(P_4)_2[Al(OR)_4]$[9] (Table 4). Anion decomposition and $(RO)_3Al–F–Al(OR)_3^-$ formation leads to new signals and a different pattern of the bands around 800 cm^{-1}.[35] The presence of a PI_2 moiety in **3** is evident from the very intense 100% band at 168 cm^{-1} which is assigned to a PI_2 stretching mode (*cf.* PI_4AlCl_4: 169 cm^{-1}, A_1 mode of PI_4^+, 100% relative intensity[36]). According to the MP2 calculation, the position of the symmetric and antisymmetric PI_2 stretches at 169 and 170 cm^{-1} are indistinguishable with the 4 cm^{-1} resolution of the spectrum and, therefore, occur at the same position which also may account for the high intensity of this band. 10 of the 15 expected vibrational bands of the cation were observed and all bands of the P_5 cage are strongly mixed. The symmetric breathing mode of the P_5 cage (A_1, 541 cm^{-1}) is slightly weakened if compared to the A_1 mode of P_4 (600 cm^{-1}) but higher in energy than the P–P vibrations of red phosphorus (highest energy band at 461 cm^{-1}).

Stability and decomposition of the $Al(OR)_4^-$ anion. Formation of 1 and 2

Previous attempts to prepare $P_2I_5^+$ salts by reaction of $I_3^+MF_6^-$ (M = As, Sb) with P_2I_4 in various solvents failed and led to

Table 3 Comparison of the ^{31}P-NMR shifts of $P_5I_2^+$ and $P_3I_6^+$ with other relevant species

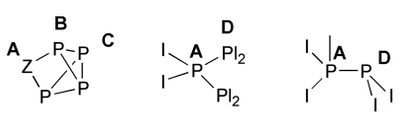

Z/Cation	δP_A	δP_B	δP_C	δP_D	$^1J(P_{AB})$	$^1J(P_{BC})$	$^1J(P_{AD})$
Cp''_2Hf[34]	—	117.5	−219.3	—	—	193.9	
Cp^*_2Zr[34]	—	93.3	−214.0	—	—	201.1	—
I_2P^+ **3**	−89.0	168.2	−193.9	—	278.5	152.6	—
$P_3I_6^+$ **4**	−4.6	—	—	89.2	—	—	385.5
$P_2I_5AlI_4$ (MAS)[22]	−142	—	—	114	—	—	—
$P_2I_5[Al(OR)_4]$[a]	−156.2	—	—	125.5	—	—	320.2

[a] From Fig. 2.

Table 4 Experimental and non-scaled calculated vibrational frequencies of **3**

$\nu_{exp.}$ [a] (% intensity)	$\nu_{calc.}$ [b]	Symmetry	Assignment
796 (21)			Al–O {*cf.* 798 in $Ag(P_4)_2[Al(OR)_4]$}
745 (20)			Al–O {*cf.* 746 in $Ag(P_4)_2[Al(OR)_4]$}
541 (32)	544	A_1	ν_s "breathing mode"of the P_5 cage
Within A_1 at 541?	537	B_1	ν_{as} P2–P1–P3
502 (20)	505	A_1	ν_s P_5 cage
Within B_1 at 448?	450	B_2	ν_{as} P2,3,1 and I1,2
448 (10)	444	B_1	ν_{as} P2,3,4,5
385 (30)	390	B_1	ν_{as} P_5 cage
359 (sh)	357	A_2	ν_{as} P2,3,4,5
354 (80)	350	A_1	ν_s P2,3,4,5
329 (70)	314	A_1	ν_{as} P_5 cage
318 (sh)			Anion {*cf.* 322 in $Ag(P_4)_2[Al(OR)_4]$}
234 (4)			Anion {*cf.* 234 in $Ag(P_4)_2[Al(OR)_4]$}
Within A_1 at 168?	170	B_1	ν_{as} PI_2 unit
168 (100)	169	A_1	ν_s PI_2 unit
126 (4)	132	B_2	P2–P1–P3 bend
87 (4)	86	A_1	PI_2 bend
n.o.	79	A_2	Cage deformation
n.o.	56	B_1	Cage deformation

[a] n.o. = not observed. [b] MP2/TZVPP frequencies.

decomposition and formation of PF_3, I_2 and MI_3.[22] The characterisation of **3** and **4** is therefore remarkable and demonstrated the stability of the $Al(OR)_4^-$ anion in comparison to the classical MF_6^- class of ions. Moreover, $Al(OR)_4^-$ salts are soluble in CH_2Cl_2 even at very low temperatures (−90 °C) which allowed the variable temperature NMR studies to be undertaken. However, at temperatures above −30 °C to rt following decomposition reactions of the $Al(OR)_4^-$ anion which led to the formation of the fluoride bridged $(RO)_3Al–F–Al(OR)_3^-$ species indicated that cations such as P_5^+ or $P_5I_2^+$ and $P_3I_6^+$ are very strong electrophiles. A possible hypothetical but balanced mechanism for the formation of the fluoride bridged anion in **1** and **2** and the subsequent insertion reactions starting from P_5^+ is outlined in Scheme 1.

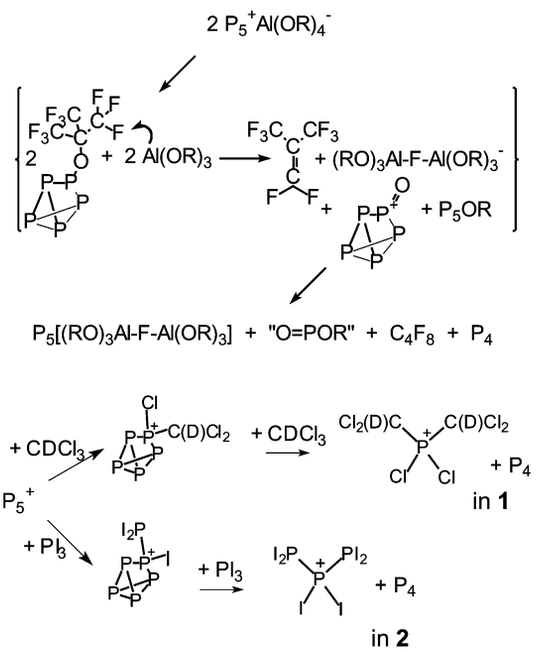

Scheme 1 Hypothetical decomposition pathway leading to **1** and **2** [R = $C(CF_3)_3$].

The first step of this decomposition reaction is possibly the abstraction of one OR ligand from $Al(OR)_4^-$. Since $Al(OR)_3$ was shown to be a very strong Lewis acid[8] and the Al–F bond is the second strongest single bond in the Periodic table [BE = 583 ± 31 kJ mol^{-1}][37] the subsequent fluoride ion abstraction from the generated P_5OR molecule close by appears likely. The fluoride ion abstraction is additionally aided by C=C (in C_4F_8) and P=O (in P_5O^+) double bond formation. In this step the fluoride bridged anion was formed. Subsequently the P_5O^+ cation reacted with additional P_5OR present giving the P_5^+ cation and other likely stable phosphorus containing species ["O=POR", *cf.* O=POH;[38] that presumably dismutates to P_2O_3 or P_2O_5, $P(OR)_3$ and P_4(or P_{red})]. The P_5^+ cation then inserted into the C–Cl bond of $CDCl_3$ (to give **1**) or PI_3 (to give **2**).

The $(RO)_3Al–F–Al(OR)_3^-$ anion has some similarity to the $Sb_2F_{11}^-$ anion. For the latter species it was shown[27] that the fluoride ion affinity (= FIA) of 2 SbF_5 (l) (giving $Sb_2F_{11}^-$) is greater than that of 1 SbF_5 (l) (giving SbF_6^-) by 70 kJ mol^{-1}. Similarly it is clear that the FIA of 2 $Al(OR)_3$ is greater than that of $Al(OR)_3$. Therefore it is likely that only the combined power of 2 $Al(OR)_3$ molecules is sufficient to abstract a fluoride ion [to form $(RO)_3Al–F–Al(OR)_3^-$ and *not* two $F–Al(OR)_3^-$ anions]. The structural parameters of the $(RO)_3Al–F–Al(OR)_3^-$ anion suggested that the fluoride bridged species is more stable (towards electrophilic attack) than the parent $Al(OR)_4^-$ ion, just as $Sb_2F_{11}^-$ is more stable than SbF_6^-.[27]

Thermodynamics of the reaction of iodine with $Ag(P_4)_2^+$, stability and formation of $Cl_2P(CHCl_2)_2^+$, $P_5I_2^+$ and $P_3I_6^+$

In Scheme 1 we proposed that the $Cl_2P(CHCl_2)_2^+$ cation was formed by the double insertion of the P^+ unit of P_5^+ into the C–Cl bond of chloroform, *i.e.*

$$P_5^+ + 2\ CHCl_3 \longrightarrow Cl_2P(CHCl_2)_2^+ + P_4 \qquad (7)$$
$$\Delta_r H = -208.2\ (\Delta_r G = -157.2)\ [MP2/TZVPP]$$

A reaction according to eqn. (7) is both exothermic and exergonic and therefore likely to be the reason for the formation of the $Cl_2P(CHCl_2)_2^+$ cation and also in agreement with the ^{31}P-NMR spectroscopic observation of excess P_4.

To understand the formation of $P_5I_2^+$ and $P_3I_6^+$ as opposed to that of P_5^+ we assessed the underlying thermochemistry in the gas phase and in solution (CS_2 and CH_2Cl_2) by including approximate free solvation energies with the COSMO model.[39] All values given include the ZPE and thermal corrections to the enthalpy (H) or the free energy (G)[40] at a temperature of 298 K [eqns. (a)–(j) in Table 5].

In the gas phase the enthalpy for the formation of P_5^+ [eqn. (a)] is unfavourable by 104.5 kJ mol^{-1}. However, including entropy, solvation energies and considering the (expected)

Table 5 MP2/TZVPP enthalpies and free energies[40] of reaction (kJ mol^{-1}) in the gas phase as well as CS_2 and CH_2Cl_2 solution (COSMO model).[39] The values in parentheses include the formation of solid AgI

Reaction	Δ_rH(gas)	$\Delta_rG(CS_2)$	$\Delta_rG(CH_2Cl_2)$
(a) $Ag(P_4)_2^+ + 3.5\ I_2 \longrightarrow P_5^+ + 2\ PI_3 + 0.25\ P_4 + AgI$	+104.5 (−92.4)[a]	+48.7 (−131.2)[b]	+14.5 (−149.4)[c]
(b) $Ag(P_4)_2^+ + 3.5\ I_2 \longrightarrow P_5I_2^+ + 4/3\ PI_3 + 5/12\ P_4 + AgI$	−19.9 (−216.9)[a]	−20.3 (−200.2)[b]	−36.8 (−200.7)[c]
(c) $P_5^+ + 2\ PI_3 \longrightarrow P_3I_6^+ + P_4$	−205.8	−101.2	−75.8
(d) $P_5^+ + I_2 \longrightarrow P_5I_2^+$	−184.8	−116.6	−98.1
(e) $P_4 + PI_2^+ \longrightarrow P_5I_2^+$	−188.6	−123.6	−113.2
(f) $P_5I_2^+ + P_2I_4 \longrightarrow P_3I_6^+ + P_4$	−49.0	−38.7	−25.7
(g) $P_2I_4 + PI_3 + Ag^+ \longrightarrow P_3I_6^+ + AgI$	−197.8 (−394.7)[a]	−140.9 (−320.8)[b]	−115.2 (−278.8)[c]
(h) $P_2I_5^+ + P_2I_4 \longrightarrow P_3I_6^+ + PI_3$	−20.3	−35.8	−32.5
(i) $P_3I_6^+ \longrightarrow P_2I_5^+ + 0.25\ P_2I_4 + 0.125\ P_4$	45.4	30.9	27.1
(j) $P_3I_6^+ \longrightarrow P_2I_5^+ + 1/3\ PI_3 + 1/6\ P_4$	53.8	29.2	25.3

[a] The enthalpy for the process AgI (g) ⟶ AgI (s) is 196.9 kJ mol^{-1}. [b] The enthalpy for the process AgI (solv) ⟶ AgI (s) in CS_2 is −179.9 kJ mol^{-1}. [c] The enthalpy for the process AgI (solv) ⟶ AgI (s) in CH_2Cl_2 is −163.6 kJ mol^{-1}.

precipitation of solid AgI (s) favours the P_5^+ side and eqn. (a) is now exergonic by −131.2 to −149.4 kJ mol^{-1}. P_5^+ formation is aided by solvation effects and more favourable in polar solvents such as CH_2Cl_2. In Scheme 1 we proposed that $P_3I_6^+$ was formed by the double insertion of the P^+ unit of P_5^+ into the P–I bond of PI_3. Eqn. (c) shows that this reaction is exergonic and therefore may be the reason for the formation of **2**. According to eqn. (b), starting with the same stoichiometry as eqn. (a), the direct formation of $P_5I_2^+$ is exergonic. $P_5I_2^+$ formation may proceed through the P_5^+ stage by reaction with excess I_2 [eqn. (d)] or alternatively through a PI_2^+ stage by insertion of the latter into the P–P bond of P_4 [eqn. (e)]. The PI_2^+ cation may have formed from Ag^+ and PI_3 which in turn originated from P_4 [from $Ag(P_4)_2^+$] and I_2. In agreement with this proposal it was shown that P_4 and I_2 initially form PI_3 and only then P_2I_4 (with excess P_4)[17] and we observed PI_3 formation in eqn. (5) above. However, solely based on thermodynamics it can not be decided whether eqn. (d), eqn. (e) or yet another pathway is actually occurring. It may be noted though that in the case of formation of the $Cl_2P(CDCl_2)_2^+$ cation in **1** a PX_2^+ insertion pathway [X = Br, I; *cf.* eqn. (e)] must be excluded since the resulting cation would have to incorporate a PBr_2^+ unit which clearly is not the case. Therefore only the intermediate participation of a phosphorus cation such as P_5^+ explains the formation of **1** [eqn. (7)] and so $P_5I_2^+$ formation as shown in eqn. (d) appears more likely, although eqn. (e) may be an alternative approach to synthesise $P_5I_2^+$.[10,41] In the *in situ* NMR reaction we observed that $P_5I_2^+$ had already decomposed at −40 °C with formation of $P_3I_6^+$. Eqn. (f) gives a reasonable explanation for this reaction: at this temperature P_2I_4, formed from PI_3 and P_4 in the precipitate, becomes slightly soluble in CH_2Cl_2 and therefore is available for a reaction with $P_5I_2^+$ giving $P_3I_6^+$ and P_4 (or P_{red} since P_2I_4 catalyses this transformation[42]). Scheme 2 summarises these findings.

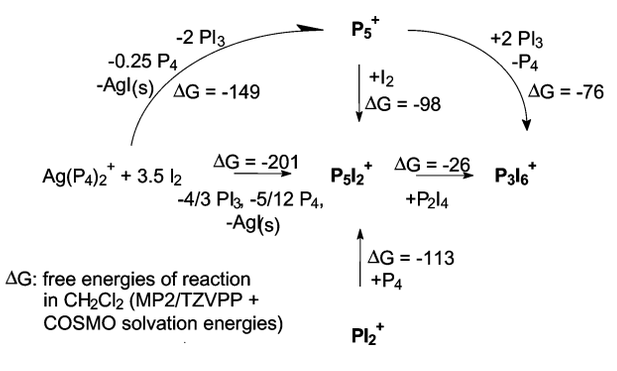

Scheme 2 The reaction of $Ag(P_4)_2^+$ with I_2 in CH_2Cl_2 solution: Likely reaction pathways. All free energies are given in kJ mol^{-1}. (s) = solid.

Eqn. (g) shows that the formation of $P_3I_6^+$ starting from phosphorus iodides and Ag^+ is thermochemically possible. Fig. 2 suggested that $P_3I_6^+$ in **4** was formed through $P_2I_5^+$, *i.e.* PI_3 reacted faster with $Ag(CH_2Cl_2)[Al(OR)_4]$ than P_2I_4 and the $P_2I_5^+$ formed reacted then with P_2I_4 to give $P_3I_6^+$ and PI_3. Eqn. (h) is in agreement with this proposal and the small exergonic reaction energy of only −32.5 kJ mol^{-1} (in CH_2Cl_2) and the low solubility of P_2I_4 in cold CH_2Cl_2 account for the slow $P_3I_6^+$ formation [eqn. (6) above]. $P_3I_6^+$ has a dynamic solution structure and coalesces at only 243 K ($\Delta G^{\#}$ = 38.8 kJ mol^{-1}). The transition state for the process that makes the two different P atoms in $P_3I_6^+$ equivalent at rt is *not* the D_{3h} symmetric three-membered ring *cyclo*-$P_3I_6^+$ owing to the high relative energy of this species [$E_{rel.}$(*cyclo*-$P_3I_6^+$) = +251 kJ mol^{-1} *vs.* C_2-$P_3I_6^+$ at the MP2/TZVPP level]. Less symmetric start geometries always led to the C_2 symmetric ground state and therefore it is most likely to assume a bimolecular exchange process for this reaction, *i.e.*:

$$2\ I_2P^A\text{–}P^BI_2\text{–}P^AI_2^+ \longrightarrow \{P_6I_{12}^{2+}\}^{\#} \longrightarrow I_2P^A\text{–}P^AI_2\text{–}P^BI_2^+\ \textit{etc.}$$

However, different or additional exchange processes such as those outlined in eqns. (i) and (j) are also likely to be involved, especially since the experimental $\Delta G^{\#}$ and $\Delta G(CH_2Cl_2)$ of eqns. (i) and (j) are on the same order of magnitude (38.8 *vs.* 25 to 27 kJ mol^{-1}).

In contrast to $P_2I_5^+$ (in $P_2I_5AlI_4$) the $P_3I_6^+$ cation was previously never observed with other anions such as AlI_4^-. Therefore we investigated the stability of **2**, **4** and a hypothetical $P_3I_6AlI_4$. Since gaseous disproportionation reactions according to eqns. (i) and (j) are still endothermic by 45 to 54 kJ mol^{-1} this process has to be governed by lattice potential enthalpies. Therefore the solid state disproportionation [eqn. (8)] was assessed with three different anions, A, by a Born–Fajans–Haber calculation[11] which showed that $P_3I_6^+$ is only stable with the large $(RO)_3$-Al–F–$Al(OR)_3^-$ anion. With $Al(OR)_4^-$ its solid state stability is slightly unfavourable.

$$P_3I_6[A]\ (s) \longrightarrow P_2I_5[A]\ (s) + 0.25\ P_2I_4\ (s) + 0.5\ P_{red}\ (s) \quad (8)$$

$$[A] = (RO)_3Al\text{–}F\text{–}Al(OR)_3\ \Delta_rH(solid) = +2.1\ kJ\ mol^{-1}$$
$$[A] = Al(OR)_4^-\ \Delta_rH(solid) = -0.9\ kJ\ mol^{-1}$$
$$[A] = AlI_4\ \Delta_rH(solid) = -10.9\ kJ\ mol^{-1}$$

Since P_4 was never observed in solution a transformation of the P_4 molecule into red phosphorus (as catalysed by phosphorus iodides)[42] was assumed which additionally favoured the right hand side of eqn. (8) by 8.85 kJ mol^{-1} (*i.e.* Δ_rH for 1/4 P_4 (s) ⟶ P_{red} (s) is 17.7 kJ mol^{-1}).[42] Eqn. (8) provided evidence for our observation that the $P_3I_6^+$ cation is only marginally stable and that—with many attempts—we were unable to obtain

single crystals of **4**. Rather **4** disproportionated giving $P_2I_5[Al(OR)_4]$[20] and P_2I_4. To obtain clean solid **4** one therefore has to quickly remove all volatiles of the diluted CH_2Cl_2 solution and the thus obtained solid **4** appears to be metastable against a disproportionation as in eqn. (8).

Conclusion

A series of reactions was performed that finally led to salts of the $P_5I_2^+$ and $P_3I_6^+$ cations. In some of the reactions the intermediate presence of naked polyphosphorus cations (*e.g.* P_5^+) as concluded from the reaction products and *ab initio* calculations appeared likely. The phosphorus atoms in $P_3I_6^+$ have an average oxidation state of 2.33 and this species is the first subvalent phosphorus P–X cation (X = H, F, Cl, Br, I) and a derivative of the as yet unknown subhalide P_3I_5 (only P_3F_5 was briefly characterised,[43] all other halides P_3X_5 are unknown). This $P_3I_6^+$ cation in **2** is only marginally stable in the solid state. The $P_5I_2^+$ cation is the first example of a binary phosphorus rich P–X cation (X = halogen, H, organyl) and shows that this class of cations is accessible if provided with a suitable robust counterion such as $Al(OR)_4^-$. Classical (oxidative) approaches to the $P_nI_m^+$ ($n \geq 2$) cations were earlier shown to be impossible since reactions always led to a complete fragmentation of the counterions MF_6^- (M = As, Sb). Moreover these classical routes only allow the isolation of oxidised but no subvalent species. This highlights the usefulness of the silver metathesis route employed here in combination with the new generation of spectator ions as exemplified by $Al(OR)_4^-$. However, the decomposition of the latter anion in solution at temperatures above −30 °C to rt showed that even more stable counterions than $Al(OR)_4^-$ are needed. The fluoride bridged $(RO)_3Al–F–Al(OR)_3^-$ anion appears to be a suitable candidate for this purpose. Currently we are investigating possible routes to the direct synthesis of silver salts of the latter anion.

Experimental

All manipulations were performed using grease free Schlenk or dry box techniques and a dinitrogen or argon atmosphere. A drawing of the employed "Single Piece Apparatus" has been deposited as ESI. All apparatus were closed by J. Young valves and the solvents were rigorously dried over P_2O_5 and degassed prior to use and stored under N_2 on molecular sieves (4 Å). Yellow phosphorus was sublimed prior to use and dissolved in CH_2Cl_2 or CS_2 giving stock solutions which were manipulated by syringe techniques. The silver aluminate $Ag(CH_2Cl_2)[Al(OR)_4]$ and $Ag(P_4)_2[Al(OR)_4]$ were prepared according to the literature.[8,9] Raman spectra were recorded on a Bruker IFS 66v spectrometer equipped with the Raman model FRA106 and were obtained in the back scattering mode from solid samples sealed in a 5 mm NMR tube (1064 nm irradiation, 4 cm^{-1} resolution). NMR spectra of sealed samples were run on a Bruker AC250 spectrometer and were referenced against the solvent (^1H, ^{13}C) or external H_3PO_4 (^{31}P) and aqueous $AlCl_3$ (^{27}Al).

Reaction leading to $Cl_2P(CDCl_2)_2^+[(RO)_3Al–F–Al(OR)_3^-]$, 1

$Ag(CH_2Cl_2)[Al(OR)_4]$ (0.101 g, 0.087 mmol) was weighed into an NMR tube and Br_2 (0.047 ml of a 0.942 M solution in CS_2, 0.0435 mmol) and P_4 (0.41 ml of a 0.266 M solution in CS_2, 0.109 mmol) were added at rt with the exclusion of light. The brownish suspension was exposed to ultrasound for 5 minutes. All volatiles were removed in vacuum and the greyish–brown residue was dissolved in 0.5 ml of $CDCl_3$ giving a brownish solution over little precipitate that appeared to be AgBr. The sample was sealed, NMR spectra were recorded and after two months a large amount of uniform colourless single crystals had formed. The unit cell of at least 10 crystals was determined and all of them were shown to be $Cl_2P(CDCl_2)_2^+[(RO)_3Al–F–Al(OR)_3^-]$, **1**, which therefore is seen as the major product of this reaction. NMR data of the solution: ^{13}C-NMR (63 MHz, $CDCl_3$, 25 °C): δ = 120.8 (q, CF_3, J_{CF} = 291.2 Hz); ^{31}P-NMR (101 MHz, $CDCl_3$, 25 °C): δ = +144 [s, $Cl_2P(CDCl_2)_2^+$, 10% of P content] −500 (s, P_4, 90% of the P content).

Reaction leading to $P_3I_6^+[(RO)_3Al–F–Al(OR)_3^-]$, 2

$Ag(CH_2Cl_2)[Al(OR)_4]$ (0.624 g, 0.522 mmol) was weighed into a single piece apparatus[44] and P_4 (1.72 ml of a 0.605 M solution in CS_2, 1.044 mmol) was added to the solid. All volatiles were removed in vacuum (slightly brownish residue). Solid I_2 (0.465 g, 1.832 mmol) was weighed into the second bulb of the apparatus, CH_2Cl_2 (10 ml) condensed onto the $P_4/Ag(CH_2Cl_2)[Al(OR)_4]$ mixture and subsequently all the iodine was sublimed onto the phosphorus containing side. The resulting orange solution over yellow precipitate was stirred overnight at −30 °C. All volatiles were removed in vacuum (theoretically expected weight of the residue: 1.174 g, found: 1.132 g) and the yellowish residue was extracted with 10 ml of CS_2 at rt. From this yellow CS_2 solution 0.501 g of a mixture of single crystals was obtained: orange needles of P_2I_4 (unit cell determination) and yellow extremely sensitive plates of $P_3I_6^+[(RO)_3Al–F–Al(OR)_3^-]$, **2** (X-ray). A Raman spectrum of this mixture only showed the bands of P_2I_4 (which in comparison to **2** is a very good Raman scatterer[18] and therefore prevents the observation of the weak $P_3I_6^+$ bands). NMR data of the CS_2 solution: ^{13}C-NMR (63 MHz, CS_2–CD_2Cl_2, 25 °C): δ = 122.2 (q, CF_3, J_{CF} = 290.6 Hz); ^{27}Al-NMR (78 MHz, CS_2–CD_2Cl_2, 25 °C): δ = 34.0 (s, $\nu_{1/2}$ = 28 Hz); ^{31}P-NMR (101 MHz, CS_2–CD_2Cl_2, 25 °C): δ = 176 ($\nu_{1/2}$ = 2100 Hz), 105 ($\nu_{1/2}$ = 1600 Hz); ^{31}P-NMR (101 MHz, CS_2–CD_2Cl_2, −30 °C): δ = 175.5 ($\nu_{1/2}$ = 5 Hz), 104.5 ($\nu_{1/2}$ = 5 Hz); ^{31}P-NMR (101 MHz, CS_2–CD_2Cl_2, −70 °C): δ = 175.7 ($\nu_{1/2}$ = 4 Hz), 103.9 ($\nu_{1/2}$ = 4 Hz).

NMR reaction leading to $P_5I_2^+[Al(OR)_4^-]$, 3

$Ag(P_4)_2^+[Al(OR)_4^-]$ (0.151 g, 0.114 mmol) was weighed into an NMR tube connected to a valve. I_2 (0.101 g, 0.399 mmol) was sublimed onto the solid at 77 K after which 0.9 ml of CD_2Cl_2 was condensed onto the mixture. The NMR tube was sealed and then placed in a dry ice–isopropanol bath and activated with ultrasound at −78 °C for about 10 minutes. The initial ^{31}P-NMR spectra were run 30 minutes later and the ^{13}C- and ^{27}Al-NMR spectra after storage at −80 °C one week later (no decomposition visible in the ^{31}P-NMR). ^{13}C-NMR (63 MHz, CD_2Cl_2, −90 °C): δ = 122.4 (q, CF_3, J_{CF} = 290.1 Hz); ^{27}Al-NMR (78 MHz, CD_2Cl_2, −90 °C): δ = 39.5 (s, $\nu_{1/2}$ = 27 Hz); ^{31}P-NMR (101 MHz, CD_2Cl_2, −90 °C): δ = 168.2 (2P, dt, $^1J_{P2,3–P1}$ = 278.5 Hz, $^1J_{P2,3–P4,5}$ = 152.6 Hz), −89.0 (1P, tt, $^1J_{P1–P2,3}$ = 278.5 Hz, $^2J_{P1–P4,5}$ = 26.7 Hz), −193.9 (2P, td, $^1J_{P4,5–P2,3}$ = 152.6 Hz, $^2J_{P4,5–P1}$ = 26.7 Hz). Upon overnight warming to −40 °C the $P_5I_2^+$ signals vanished and, apart from other unassigned signals of lower intensity, those of $P_3I_6^+$ appeared as the major P-containing peaks [$\delta^{31}P$(−80 °C) = 89.2 (2P, d, $^1J_{pp}$ = 385.5 Hz), −4.6 (1P, t, $^1J_{pp}$ = 385.5 Hz)].

Synthesis of $P_5I_2^+[Al(OR)_4^-]$, 3

$Ag(P_4)_2^+[Al(OR)_4^-]$ (1.020 g, 0.765 mmol) was weighed into a two bulbed vessel incorporating a sintered glass frit and stopped by J. Young valves. I_2 (0.697 g, 2.746 mmol) was sublimed onto the solid at 77 K after which 5 ml of CH_2Cl_2 were condensed onto the mixture. The apparatus was placed in a dry ice–isopropanol bath until the solvent had thawed and was then stored in a −80 °C freezer and every 30 minutes heavily shaken for about one minute (10 times). After four days at −80 °C the yellow solution over a yellow–orange precipitate was filtered at −80 °C. All volatiles were then quickly removed at about 0 °C (expected weight of the material: 1.717 g, found: 1.737 g) and

the apparatus immediately transferred into a glove box. Soluble yellow $P_5I_2^+[Al(OR)_4^-]$, **3** [0.963 g (0.700 mmol), expected: 1.052 g; yield: 92%] and 0.611 g insoluble material (expected: 0.665 g) were isolated while 0.140 g were not accessible within the flask (total: 0.963 g + 0.611 g + 0.140 g = 1.714 g; expected: 1.717 g). Raman spectra of **3** (see Table 4) and the insoluble material (P_4, PI_3 and traces of P_2I_4) were recorded immediately after sample preparation. A ^{31}P-NMR sample of yellow **3** in CD_2Cl_2 gave the same spectrum as the one observed in the *in situ* reaction above. Elemental analysis for $P_5I_2^+[Al(OR)_4^-]$ ($C_{16}Al_1F_{36}I_2O_4P_5$): found I 18.7, calc. I 18.5%.

NMR scale synthesis of $P_3I_6^+[Al(OR)_4^-]$, 4

$Ag(CH_2Cl_2)[Al(OR)_4]$ (0.110 g, 0.095 mmol), PI_3 (0.040 g, 0.097 mmol) and P_2I_4 (0.054 g, 0.095 mmol) were weighed into a NMR tube attached to a valve. 1.0 ml of CD_2Cl_2 was condensed onto the mixture at 77 K and the tube was flame sealed *in vacuo*. Upon warming an orange solution and AgI precipitate formed at low temperatures. The mixture was heavily shaken for 15 minutes after which all visible phosphorus iodides were consumed. The tube was than stored at −78 °C until the NMR spectra were recorded 12 h later ($P_2I_5^+$ and $P_3I_6^+$ present). Another NMR run after 14 d storage at −30 °C showed that only $P_3I_6^+$ was present (NMR data given in text).

Synthesis of $P_3I_6^+[Al(OR)_4^-]$, 4

PI_3 (0.205 g, 0.498 mmol), P_2I_4 (0.286 g, 0.502 mmol) and CH_2Cl_2 (5 ml) were added into one bulb of a single piece apparatus.[44] This mixture was cooled to −78 °C when $Ag(CH_2Cl_2)[Al(OR)_4]$ (11.3 ml of a 0.0443 M solution in CH_2Cl_2, 0.500 mmol) were slowly added. An orange solution and AgI precipitate formed at low temperatures (−78 °C). The stirred mixture was allowed to reach room temperature within 30 minutes and after an additional 30 minutes all visible phosphorus iodides were consumed. The apparatus was then stored for 4 days at −30 °C after which a ^{31}P-NMR sample of the solution was prepared from a special outlet. This NMR spectrum showed $P_3I_6^+$ to be the only P-containing species present and, therefore, the mixture was filtered. The insoluble precipitate (AgI, found: 0.120 g, calc.: 0.117 g) was washed several times (back condensing of CH_2Cl_2) and then all volatiles of the filtrate were quickly removed *in vacuo* leaving a yellow powder of **4** (0.724 g, 79%). Raman samples prepared from this powder rapidly decomposed in the beam of the laser with all conditions checked. NMR data and analysis of yellow **4** in CD_2Cl_2: ^{13}C-NMR (63 MHz, CD_2Cl_2, 25 °C): δ = 121.5 (q, CF_3, J_{CF} = 292.1 Hz); ^{27}Al-NMR (78 MHz, CD_2Cl_2, 25 °C): δ = 36.0 (s, $\nu_{1/2}$ = 22 Hz); ^{31}P-NMR (101 MHz, CD_2Cl_2, 25 °C): δ = 61 ($\nu_{1/2}$ = 1000 Hz) ^{31}P-NMR (101 MHz, CD_2Cl_2, −90 °C): δ = 89.2 (d, $^1J_{PP}$ = 385.5 Hz, 2 P), −4.6 (t, $^1J_{PP}$ = 385.5 Hz, 1 P). $C_{16}Al_1F_{36}I_6O_4P_3$: found I 41.4, calc. I 41.8%.

X-Ray crystal structure determinations

Data collections for X-ray structure determinations were performed on a STOE IPDS diffractometer using graphite-monochromated Mo-Kα (0.71073 Å) radiation. Single crystals were mounted in perfluoroether oil on top of a glass fibre and then brought into the cold stream of a low temperature device so that the oil solidified. Crystals of **2** given to cooled (−20 °C) dry perfluoroether or hydrocarbon oil decomposed very rapidly and from the fluorinated oil one had about 45 to 60 seconds to select a crystal, put it on top of the glass fibre and bring it onto the diffractometer. Of the approximately 15 crystals tested the one reported gave the best data set. All calculations were performed on PC's using the SHELX97 software package.[50] The structures were solved by direct methods and successive interpretation of the difference Fourier maps, followed by least-squares refinement. All atoms were refined anisotropically. The $P_3I_6^+$ cation in **2** is disordered over two positions (0.865 to 0.135 occupancy) and only the major position is discussed in the text. The anions in **1**–**2** exhibit rotational disorder of the CF_3 groups as well as the entire $C(CF_3)_3$ groups. Therefore several fluorine and carbon atoms were split over two positions resulting in site occupation factors of 20–40%. Moreover a series of about 233 (**1**)/177 (**2**) SADI and FREE restraints had to be used in both structures to assign reasonable structural parameters to the CF_3 groups. However, the cations in **1**–**2** were well behaved. The solid state packing of **2** was drawn with Diamond 2.1 (K. Brandenburg, Crystal Impact GbR, 1998). Relevant data concerning crystallography, data collection and refinement details are compiled in Table 6.

Table 6 Crystallographic data and refinement details

Compound	**1**	**2**
Crystal size/mm	0.3 × 0.4 × 0.5	0.05 × 0.3 × 0.3
Formula	$C_{26}H_2Al_2Cl_6F_{55}O_6P$	$C_{24}Al_2F_{55}I_6O_6P_3$
Formula weight	1752.91	2337.51
Crystal system	Triclinic	Triclinic
Space group	$P\bar{1}$	$P\bar{1}$
a/Å	12.781(3)	10.375(2)
b/Å	13.445(3)	10.757(2)
c/Å	16.561(3)	26.591(5)
α/°	88.45(3)	95.07(3)
β/°	69.56(3)	92.84(3)
γ/°	82.99(3)	98.48(3)
V/Å^3	2646.3(9)	2917.6(10)
Z	2	2
ρ(calc)/Mg m^{-3}	2.200	2.661
μ/mm^{-1}	0.625	3.521
Max./min. transmission	0.678/0.746	0.832/0.873
2θ/°	51.84	51.90
T/K	170	175
Reflections collected	20542	18169
Reflections unique	9396	10614
Reflections observed (4σ)	6929	2630
R(int)	0.0415	0.1850
GOOF	1.087	0.676
Final R (4σ)	0.1298	0.0744
Final $wR2$	0.3729	0.1636
Largest residual peak/e Å^{-3}	1.339	1.088

CCDC reference numbers 162636 and 162637.

See http://www.rsc.org/suppdata/dt/b1/b103957c/ for crystallographic data in CIF or other electronic format.

Computational details

Initial calculations and the calculation of the thermal contributions to the enthalpy and free energy were performed with Gaussian98.[45] For P the 6-311G(2df) basis set was used and for I the SDD effective core potential augmented with one set of uncontracted s, p, d and f polarisation functions [= SDD-(spdf)]. Since it was realised that MP2 geometries were needed to give an accurate description of the species in question all further computations were done with the program TURBOMOLE.[46] The geometries of all species were optimised at the (RI-)MP2 level[47] with the triple ζ valence polarisation (one d and one f function) TZVPP basis set.[48] The 46 core electrons of I were replaced by a quasi-relativistic effective core potential. Approximate solvation energies (CS_2 and CH_2Cl_2 solution with ε_r = 2.63 and 8.92) were calculated with the COSMO model[49] at the BP86/SV(P) (DFT-)level using the MP2/TZVPP geometries. Frequency calculations were performed for all species and all structures represent true minima without imaginary frequencies on the respective hypersurface. For thermodynamic calculations the zero point energy and thermal contributions to the enthalpy or the free energy at 298 K have been included.[40] For selected species a modified Roby–Davidson population analysis has been performed using the MP2/TZVPP electron density.

Acknowledgements

We thank Prof. H. Schnöckel and Prof. J. Passmore for valuable discussions and advice, Dipl. Chem. G. Stößer and Dipl. Chem. J. Bahlo for recording the Raman spectra and H. Berberich and Dr. E. Matern for recording the many low temperature NMR spectra. Financial support from the German science foundation DFG and the Fond der Chemischen Industrie are gratefully acknowledged.

References and notes

1 (*a*) T. P. Martin, *Z. Phys. D: At., Mol. Clusters*, 1986, **3**, 211; (*b*) R. Huang, H. Li, Z. Lin and S. Yang, *J. Phys. Chem.*, 1995, **99**, 1418; (*c*) R. B. Huang, Z. Y. Liu, P. Zhang, Y. B. Zhu, F. C. Lin, J. H. Zhao and L. S. Zheng, *Chin. J. Struct. Chem.*, 1993, 180; (*d*) Z. Y. Liu, R. B. Huang and L. S. Zheng, *Z. Phys. D: At., Mol. Clusters*, 1996, **38**, 171.

2 J. A. Zimmerman, S. B. H. Bach, C. H. Watson and J. R. Eyler, *J. Phys. Chem.*, 1990, **95**, 98.

3 L.-S. Wang, B. Niu, Y. T. Lee and D. A. Shirley, *J. Chem. Phys.*, 1990, **93**, 6318.

4 (*a*) P_n and P_n^+, n = 1–8, R. O. Jones and D. Hohl, *J. Chem. Phys.*, 1990, **92**, 6710; (*b*) P_n and P_n^+, n = 1–11, R. O. Jones and G. Seifert, *J. Chem. Phys.*, 1992, **96**, 7564; (*c*) E_n and E_n^+, n = 1–11, E = P, As, R. O. Jones and P. Ballone, *J. Chem. Phys.*, 1994, **100**, 4941.

5 See for example: (*a*) D. D. Wagman, W. H. Evans, V. B. Parker, R. H. Schumm, I. Halow, S. M. Bailey, K. L. Churney and R. L. Nuttal, *J. Phys. Chem. Ref. Data, Suppl.*, 1982, **11**, 2; (*b*) S. G. Lias, J. E. Bartmess, J. F. Liebman, J. L. Holmes, R. D. Levin and W. G. Mallard, *J. Phys. Chem. Ref. Data, Suppl.*, 1988, **17**, 1; (*c*) *CRC Handbook of Chemistry and Physics*, 76th edn., editor-in-chief D. R. Lide, CRC Press, Boca Raton, FL, 1986; (*d*) http://www.nist.gov/chemistry.

6 J. D. Corbett, in *Progress in Inorganic Chemistry*, vol. 21, editor S. J. Lippard, John Wiley, New York, 1976, pp. 129–158.

7 S. M. Ivanova, B. G. Nolan, Y. Kobayashi, S. M. Miller, O. P. Anderson and S. H. Strauss, *Chem. Eur. J.*, 2001, **7**, 503.

8 I. Krossing, *Chem. Eur. J.*, 2001, **7**, 490.

9 (*a*) I. Krossing, *J. Am. Chem. Soc.*, 2001, **123**, 4603; (*b*) I. Krossing and L. van Wüllen, *Chem. Eur. J.*, 2002, **8**, 700.

10 I. Krossing and I. Raabe, *Angew. Chem.*, 2001, **113**, 4544.

11 Data employed for the Born–Fajans–Haber cycle calculations (all enthalpies in kJ mol^{-1}): (*a*) Lattice potential enthalpies were taken from the literature (AgI: 890.3)[5c] or estimated by Jenkins and Passmore's volume based modified Kapustinskii equation:[12] $Ag[Al(OR)_4]$ = 364, $P_5[Al(OR)_4]$ = 345, $P_3I_6[Al(OR)_4]$ = 334, $P_2I_5[Al(OR)_4]$ = 340, $P_3I_6[(RO)_3Al–F–Al(OR)_3]$ = 311, $P_2I_5[(RO)_3Al–F–Al(OR)_3]$ = 314, $P_2I_5[AlI_4]$ = 398, $P_3I_6[AlI_4]$ = 386. The thermochemical volume of $Al(OR)_4^-$ is 725 $Å^3$, Ag^+ (4 $Å^3$), AlI_4^- (244 $Å^3$). The volumes of P_5^+ [≈120 $Å^3$, with $S_3N_2^+(97) < P_5^+ < S_3Cl_3^+(146)$],[12] $P_2I_5^+$ [=261 $Å^3$, from $V(P_2I_5AlI_4) = 505$[21] and $V(AlI_4^-)$ above], $P_3I_6^+$ [≈330 $Å^3$, with $V(P_3I_6^+) \approx 1.5*V(P_2I_4)$] and $(RO)_3Al–F–Al(OR)_3^-$ [=1129 $Å^3$, from $V(P_3I_6[(RO)_3Al–F–Al(OR)_3]) = 1459$ and $V(P_3I_6^+)$ above] were assessed/estimated; (*b*) Enthalpies of sublimation were taken from the literature (P_4: 54.4, I_2: 62.4) or were assessed [P_2I_4: $\Delta H_{subl}(P_2I_4) = 83.0$; by computing the enthalpy of reaction for the process: 0.5 P_4 (g) + 2 I_2 (g) ⟶ P_2I_4 (g); $\Delta_f H$ = −156.7 at the MP2/TZVPP level. $\Delta_f H(P_4\,(g))$, $\Delta_f H(I_2\,(g))$ (see below) and $\Delta_f H(P_2I_4\,(s)) = -87.7$ are known]; (*c*) Enthalpies of formation were taken from the literature (Ag^+ (g): 1017, I^- (g): −188.6, P_4 (g): 54.4, I_2 (g): 62.4, P_3^+ (g): 1006, AgI (g): 135) or assessed (P_2I_4 (g): −4.7, MP2/TZVPP see above; P_5^+ (g): 913; see text).

12 H. K. Roobottom, H. D. B. Jenkins, J. Passmore and L. Glasser, *Inorg. Chem.*, 1999, **38**, 3609.

13 We optimised the known[4] global minima of the P_n^+ cations (n = 3, 5, 7) at the BP86/SVP, B3LYP/TZVPP and MP2/TZVPP levels and also calculated the vibrational frequencies and Raman intensities (only BP86) of these species. The observed new P–P stretches (480 to 630 cm^{-1}) fell into a range calculated to be typical for these cations.

14 Zdirad Zak and M. Cernik, *Acta Crystallogr., Sect. C*, 1996, **52**, 290.

15 Similarly CS_2 was used to remove excess S_8 in highly electrophilic and oxidising sulfur cation or S_2N^+ chemistry.

16 We showed that solid P_4 is also visible in a conventional solution NMR spectrometer due to the high local symmetry of the cubic solid P_4 (see ref. 9***b***).

17 B. W. Tattershall and N. L. Kendall, *Polyhedron*, 1994, **13**, 1517.

18 As observed earlier, large counterions such as $Al(OR)_4^-$ lead to fluorescence and dilute the amount of Raman scatterer present (= number of scattering $P_5I_2^+$ cations per volume). Therefore the intensity of the signals in the spectrum is low. For comparison: the 100% peak in the Raman spectrum of **3** spans only 0.1 Raman units while P_4 and PI_3 with the same conditions (laser power, sample sealed in NMR tube) have intensities of 3.0 to 5.0 Raman units for their 100% bands. This shows that already very small impurities of P_4, PI_3 or other intense Raman scatterers show in the obtained spectrum.

19 Excess P_2I_4 is insoluble at −90 °C and, therefore, invisible in the ^{31}P-NMR at −90 °C.

20 We could independently verify this assignment by directly synthesising and characterising $P_2I_5[Al(OR)_4]$. We found that $P_2I_5^+[Al(OR)_4]^-$ is rapidly formed from 2 PI_3 and $Ag(CH_2Cl_2)$-$[Al(OR)_4]$, however, this is subject to ongoing research and will be published elsewhere.

21 S. Pohl, *Z. Anorg. Allg. Chem.*, 1983, **498**, 20.

22 C. Aubauer, G. Engelhardt, T. M. Klapötke and A. Schulz, *J. Chem. Soc., Dalton Trans.*, 1999, 1729.

23 M. Hesse, H. Maier and B. Zeeh, *Spektroskopische Methoden in der Organischen Chemie*, 4th edn., 1991, Georg Thieme Verlag, Stuttgart–New York, p. 96.

24 Although many crystals were tried and three full data sets were recorded at 170 K none of them gave a fully satisfactory result and the agreement factors were never better than 12.98%. However, the crystal system and space group are well determined and the thermal ellipsoids are normal. All trace electron density (about 1.0 to 1.3 e $Å^{-3}$) appeared in the vicinity of the 18 CF_3 groups which suggested manifold rotational disorder as the reason for the bad agreement factors.

25 The $Cl_2P(CHCl_2)_2^+$ cation was fully optimised in C_2 symmetry at the MP2/TZVPP level and all structural parameters of the cation in **1** could be reproduced in the gas phase within +0.02 Å and ±1°, *i.e.* P–Cl = 1.953 Å, P–C = 1.830 Å, C–Cl = 1.751, 1.758 Å, Cl–P–Cl = 110.9°, C–P–C = 110.4°. For energies see ref. 26.

26 For the geometry of $Cl_2P(CHCl_2)_2^+$ see ref. 25; total energy: −3176.10253 a.u., ZPE: 0.04672, *G*: −0.00544. $CHCl_3$ (C_{3v}): *d*(C–H) = 1.087 Å; *d*(C–Cl) = 1.763 Å, total energy: −1417.71307 a.u.; ZPE = 0.02027, *G* = −0.01092.

27 S. Brownridge, H. D. B. Jenkins, I. Krossing, J. Passmore and H. K. Roobottom, *Coord. Chem. Rev.*, 2000, **197**, 397.

28 J. A. Zimmerman, S. B. H. Bach, C. H. Watson and J. R. Eyler, *J. Chem. Phys.*, 1990, **95**, 98.

29 It was shown convincingly that iodine substituents at tetracoordinate phosphorus atoms lead to a very pronounced upfield shift due to relativistic spin–orbit coupling mediated to the nucleus by an effective Fermi contact mechanism.[30] Therefore only relativistic ^{31}P-NMR shifts give meaningful answers as may be illustrated by the calculated non relativistic (NR) and relativistic (R) chemical shift of PI_4^+[30] which differ by over 700 ppm: $\delta^{31}P_{NR}$ = +211 and $\delta^{31}P_{NR}$ = −520! At present no routine for the standard calculation of relativistic NMR shifts is implemented in the current program codes.

30 M. Kaupp, C. Aubauer, G. Engelhardt, T. M. Klapötke and O. Malkina, *J. Chem. Phys.*, 1999, **110**, 3897.

31 A search of the chemical abstracts data base with Scifinder and the Cambridge structural database CSD with the program Conquest did not reveal a precedent for this P_5-cage. However, similar C_{2v} symmetric MP_4 units (*i.e.* M = Zr, Hf) formally containing a P_4^{2-} unit are known (see ref. 34).

32 The chemical shifts of the naked or solvated P_5^+ cation can be meaningfully computed since it bears no heavy iodine atoms.

33 If not restrained by symmetry, the calculations always lead to C_{4v}-P_5^+. Species containing C_{4v}-P_5^+ (and solvates) are true minima without imaginary frequencies and are lower in relative energy.

34 O. J. Scherer, M. Swarowsky and G. Wolmershäuser, *Angew. Chem., Int. Ed. Engl.*, 1988, **27**, 694.

35 I. Krossing, Habilitation thesis, University of Karlsruhe, 2002.

36 C. Aubauer, M. Kaupp, T. M. Klapötke, H. Nöth, H. Pietrowski, W. Schnick and J. Senker, *J. Chem. Soc., Dalton Trans.*, 2001, 1880.

37 J. E. Huheey, *Inorganic Chemistry*, 4th edn., Harper and Collins, New York, 1993.

38 H. Schnöckel and S. Schunck, *Phosphorus, Sulfur, Silicon Relat. Elem.*, 1988, **39**, 89.

39 Solvation energies were obtained from the MP2/TZVPP geometries using the COSMO model at the BP86/SVP level and dielectric constants for CS_2 and CH_2Cl_2 of 2.63 and 8.92 respectively.

40 Thermal and entropic contributions to the enthalpy and free energy were obtained by fully optimising all the species in question with Gaussian98W at the semiempirical PM3 level. All these species also represented true minima without imaginary frequencies at the PM3 level. ZPE's were taken from the MP2 calculation. Since statistical

thermodynamics is only little influenced by the employed geometries and the entropic contributions mainly arise from the moment of inertia of a species, it is believed that errors associated with this procedure are very small if used consistently.
41 In agreement with this we succeeded in the preparation of $P_5Br_2^+$ by reacting PBr_3, P_4 and $Ag(CH_2Cl_2)[Al(OR)_4]$ in CH_2Cl_2 (X-ray, Raman, NMR). However, this is subject to ongoing research and will be published elsewhere. A preliminary account appeared in *Angew. Chem.* (see ref. 10).
42 A. F. Holleman, E. Wiberg and N. Wiberg, *Lehrbuch der Anorganischen Chemie*, 101st edn., Walter de Gruyter, Berlin–New York, 1995, p. 1255.
43 D. Solan, *U. S. C. F. S. T. I. PB Rep.*, 1969, (PB-187819), p. 247; From *US Gov. Res. Dev. Rep.*, 1970, **70**, 61.
44 This U-shaped apparatus incorporates two bulbs stopped with J. Young valves. Both bulbs are connected by a glass tube including a fine sintered glass frit and the product side also included an additional valve that allowed the direct preparation of NMR samples of the reaction solution.
45 Gaussian 98, Revision A.3, Gaussian, Inc., Pittsburgh, PA, 1998.
46 TURBOMOLE, Version 5; (*a*) R. Ahlrichs, M. Bär, M. Häser, H. Horn and C. Kölmel, *Chem. Phys. Lett.*, 1989, **162**, 165; (*b*) M. v. Arnim and R. Ahlrichs, *J. Chem. Phys.*, 1999, **111**, 9183.
47 F. Weigend and M. Häser, *Theor. Chim. Acta*, 1997, **97**, 331.
48 (*a*) A. Schäfer, H. Horn and R. Ahlrichs, *J. Chem. Phys.*, 1992, **97**, 2571; (*b*) A. Schäfer, C. Huber and R. Ahlrichs, *J. Chem. Phys.*, 1994, **100**, 5829.
49 A. Klamt and G. Schürmann, *J. Chem. Soc., Perkin. Trans. 2*, 1993, 799.
50 G. M. Sheldrick, SHELX97, Program for crystal structure determination, University of Göttingen, Germany, 1997.